Journal of Materials Science & Technology 97 (2022) 29–37

Contents lists available at ScienceDirect

Journal of Materials Science & Technology

journal homepage: www.elsevier.com/locate/jmst

Research Article

Insights on high temperature friction mechanism of multilayer ta-C films

Jing Wei[a], Peng Guo[a], Hao Li[a,b], Peiling Ke[a,b], Aiying Wang[a,b,c,*]

[a] Key Laboratory of Marine Materials and Related Technologies, Zhejiang Key Laboratory of Marine Materials and Protective Technologies, Ningbo Institute of Materials Technology and Engineering, Chinese Academy of Sciences, Ningbo 315201, China
[b] Center of Materials Science and Optoelectronics Engineering, University of Chinese Academy of Sciences, Beijing 100049, China
[c] Ningbo Institute of Industrial Technology, Ningbo 315201, China

ARTICLE INFO

Article history:
Received 24 December 2020
Revised 9 March 2021
Accepted 14 April 2021
Available online 15 June 2021

Keywords:
Tetrahedral amorphous carbon
Multilayer structure
High temperature friction
Wear mechanism

ABSTRACT

In this work, the high temperature friction mechanism of the tetrahedral amorphous carbon (ta-C) film was elucidated. The multilayer ta-C film with alternating hard and soft sub-layers exhibited a low friction coefficient of 0.14 at 400 °C before a sudden failure occurred at 4600 cycles. The wear failure was attributed to the gradual consumption of the ta-C film at the contact region. The design of a hard or soft top layer effectively regulated the high temperature friction properties of the multilayer ta-C. The addition of a hard top layer contributed to a low friction coefficient (0.11) and a minor wear rate (4.0×10^{-7} mm^3/(N m)), while a soft top layer deteriorated the lubrication effect. It was proposed that the passivation of dangling bonds at the sliding interface dominated the low-friction mechanism of the ta-C film at high temperature, while the friction induced graphitization and the formation of sp^2-rich carbonaceous transfer layer triggered C–C inter-film bonding, resulting in serious adhesion force and lubrication failure. Moreover, the multilayer ta-C film with hard top layer obtained excellent friction performance within 500 °C, while the high temperature induced oxidation and volatilization of carbon atoms led to the wear failure at 600 °C.

1. Introduction

Inspired by natural substances, such as bones and sea shells, layer-by-layer assembled structure is expected to endow materials with outstanding mechanical properties [1,2]. The regular stacking of hard and soft components may exert synergistic effects and achieve hard yet tough materials, providing novel vision for material design.

Previously, tetrahedral amorphous carbon (ta-C) was explored in constructing laminated nano-architecture consisting of alternate hard and soft sub-layer [3–6]. The multilayer structure could effectively relieve the residual stress stemmed from the bombardment of energetic particles during growth [7], which is a major concern for ta-C film. Compared to the element doping and post-annealing [8–10], the hard and soft layer alternated multilayer structure slightly sacrificed the mechanical properties of ta-C film.

The friction performance of the multilayer ta-C film was closely related to the structure design. The modulation ratio and components of adjacent sub-layer could tailor the wear resistance, which mainly originated from the variation in hardness, toughness, or balance between hardness and residual stress [7,11–14]. Moreover, the top layer of the multilayer structure dominated the wear behavior at high contact pressure [15,16]. A soft top layer benefited the anti-wear performance of carbon/carbon multilayer film at high contact stress owing to the rapid formation of transfer layer during the run-in period [15]. In our previous work [12], the dry friction behaviors of the multilayer ta-C film with different adjacent layer was closely associated with the ratio of hardness to elastic modulus.

In reality, the harsh application environment is not limited to the threat of mechanical loads. Various application fields including thermal assisted magnetic storage [17,18], machining of Al alloy [19] and glass molding [20] simultaneously involve mechanical load and high temperature (300–700 °C), which poses a great challenge for the ta-C protective coating. At present, the high temperature behaviors of the ta-C film have been reported [21–24]. Deng et al. [21] proposed that the degraded friction performance of ta-C film exceeded 400 °C was contributed to the deteriora-

* Corresponding author at: Key Laboratory of Marine Materials and Related Technologies, Zhejiang Key Laboratory of Marine Materials and Protective Technologies, Ningbo Institute of Materials Technology and Engineering, Chinese Academy of Sciences, Ningbo 315201, China.
E-mail address: aywang@nimte.ac.cn (A. Wang).

https://doi.org/10.1016/j.jmst.2021.04.028
1005-0302/

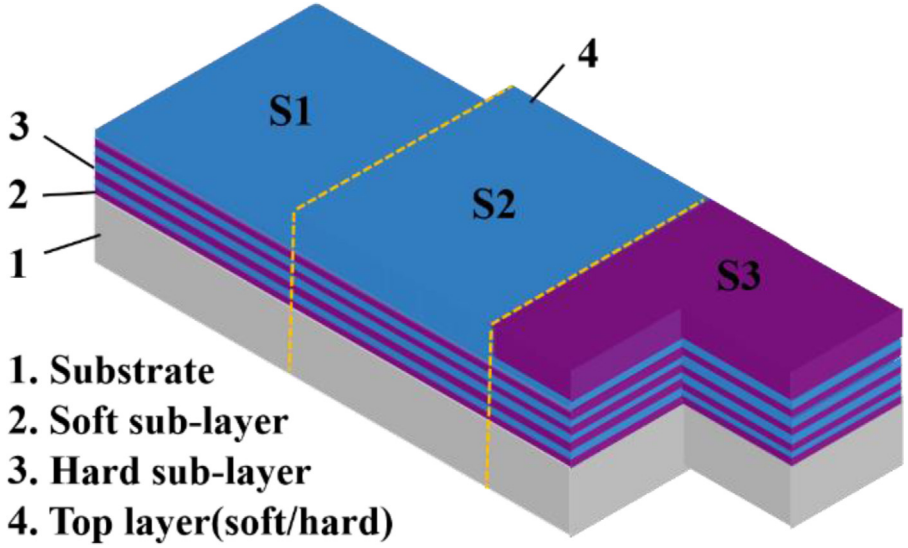

Fig. 1. Structure diagram of the multilayer ta-C films.

tion of toughness, in which the increase of crack nucleation position and crack growth led to serious film delamination. Bhowmick et al. [22] found that a-C and ta-C-F friction pairs could maintain a low friction coefficient (0.1–0.2) at 300 °C, which originated from the formation of fluorine-containing carbon transfer layer and the passivation of carbon atoms on the contact surface. Miyake et al. [24] found that the durability of the ultra-thin ta-C film decreased at temperature higher than 300 °C due to the complex action of friction and high temperature. It was concluded that the ta-C film maintained a good friction performance within 400 °C, which failed to meet the demand of special fields with higher temperature. More importantly, there is little research on the high temperature friction performance of multilayer ta-C film, and its high temperature friction mechanism remains unclear. Compared with room temperature friction, the positive effects of graphitized transfer film at high temperature is questionable, in which serious adhesion may occur.

The main purpose of this work was to investigate the friction mechanism of the multilayer ta-C at high temperature. The structure of the aforementioned multilayer ta-C film in our previous work was optimized by top-layer design, where a hard top layer (sp^3-rich layer) or a soft top layer (sp^2-rich layer) was added. The results could benefit the deep insight into the wear mechanism of ta-C film at high temperature and provide guidance for the high temperature-oriented applications of ta-C film.

2. Experimental

Multilayer ta-C films were fabricated by a home-made 45° double-bent filtered cathodic vacuum arc (FCVA) system, using YG8 cemented carbide with 26 mm in diameter as substrates. As reported in our previous work [12], the four period multilayer ta-C was realized by alternating the high bias voltage of −150 V and low bias voltage of −50 V, and the modulation ratio was 1:1. Besides the previous multilayer ta-C film, a hard top layer (sp^3-rich layer) or a soft top layer (sp^2-rich layer) was deposited on the previous multilayer structure at bias voltage of −50 V and −150 V, respectively. The hardness of the hard and soft top layer measured by nano-indentation tests were 55.2 GPa and 36.7 GPa, respectively (as shown in Table S1 in the Supporting Information). Fig. 1 shows the structure diagram of the three kinds of multilayer ta-C films. The deposition system and fabrication processes were carefully described in the previous work. The thickness of the hard/soft top layer was controlled at about 120 nm by changing the deposition time. The specific parameters were shown in Table 1, and the samples were labeled as S1-S3 according to the structural design.

A high temperature rotating ball-on-disk tribometer (Anton Paar, THT) was employed to acquire the coefficients of friction (COF) and wear rates of the multilayer ta-C films at an applied load of 2 N for 10,500 revolutions. The counterparts were Al_2O_3 balls with the diameter of 6 mm. Friction tests were conducted at sliding velocity of 5 cm/s and sliding radius of 3 mm. The test temperatures were 400, 500 and 600 °C. The cross-sectional profiles of the wear tracks were characterized by a surface profilometer (Alpha Step-IQ), and the profiles were measured for five times to improve accuracy. The wear rates were calculated by the Eq. (1):

$$K = V/FL \tag{1}$$

where V is the wear volume loss (mm^3), F is the normal load (N), L is the sliding distance (m). The wear volumes of the films were acquired by the Eq. (2) [25]:

$$V_{film} = 2\pi R \times S \tag{2}$$

where R is the friction radius (mm), S is the cross-sectional area of the wear track (mm^2). The wear volumes of the counterpart balls were determined by the Eqs. (3)-(4) [26]:

$$V_{ball} = \pi h/6 \times \left(3d^2/4 + h^2\right) \tag{3}$$

$$h = r - \left(r^2 - d^2/4\right)^{1/2} \tag{4}$$

where d is the diameter of the wear scar (mm), r is the radius of the counterpart balls (mm). The wear tracks on ta-C and wear scars on Al_2O_3 ball were comprehensively evaluated by a scanning electron microscopy (SEM, FEI Quanta FEG 250), and the areal distributions of Al, O, C, W and Co elements on the Al_2O_3 counterpart were ascertained by energy dispersive X-ray spectroscopy (EDS). An optical microscope (LSM700) was utilized to acquire the surface morphologies of the contact areas, and the typical positions on the wear tracks and wear scars were analyzed by the Raman spectroscopy with laser wavelength of 532 nm (Renishaw inVia-reflex, UK).

The post-annealing treatment was conducted in a tube furnace with annealing temperature of 400, 500 and 600 °C. After annealing for 30 min, the samples were naturally cooled down. The evolution of chemical composition and carbon atomic bonds were analyzed by the X-ray photoelectron spectroscopy (XPS, Axis ultradld,

Table. 1
Specific parameters of the designed multilayer ta-C films.

Samples	Alternated bias voltage (V)	Bias of top layer (V)	Total thickness(nm)
S1	−150/−50	/	245
S2	−150/−50	−50 (hard)	360
S3	−150/−50	−150 (soft)	368

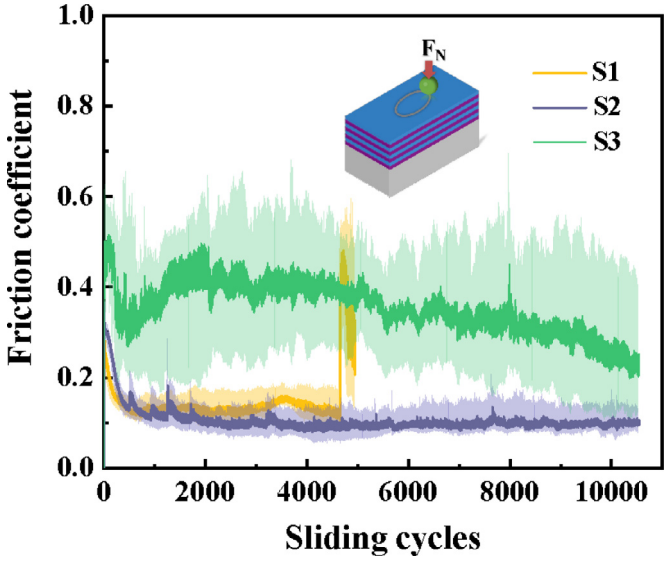

Fig. 2. Friction curves of multilayer ta-C films at 400 °C (Inset shows the schematic diagram of the friction test).

Japan) using a monochromatic Al X-ray source. The XPS apparatus had an energy resolution of 0.48 eV. The C 1s peak at 284.6 eV was used to calibrate the binding energy.

3. Results and discussion

The friction tests of ta-C films sliding against Al_2O_3 counterpart at 400 °C were carried out to elucidate the role of top layer in the high temperature friction behaviors. Fig. 2 shows the typical evolution of the friction coefficient against sliding cycles. The friction coefficients of all the samples firstly exhibited a downward trend, revealing a run-in process. The S1 film exhibited a friction coefficient of 0.12 before a sudden increase at 4600 cycles, which indicated that it was worn out. After sliding for about 500 cycles, the S2 film obtained a stable friction curve and a low friction coefficient of 0.11. The friction curve of the S3 film fluctuated evidently during the friction test, and its friction coefficient after run-in stage increased rapidly from 0.30 to 0.45, and then gradually decreased to 0.21. Therefore, the addition of a hard top layer contributed to improved friction performance of the multilayer ta-C at 400 °C, while a soft top layer surprisingly deteriorated the friction behavior.

Fig. 3 shows the representative SEM surface morphologies and cross-section profiles of the wear tracks on the multilayer ta-C films. Wear track, with width 117 μm and depth 282 nm, was observed on the S1 film, and local peeling was noticed at the edge of the wear track, indicating a severe damage. The wear of the S2 film was mild that the wear track was barely discernible. The wear track of the S3 film was 75 μm in width and 107 nm in depth, which was comparable to that of S2 film. However, the degree of wear was unevenly distributed on the wear track of the S3 film, and the deep grooves implied the possible occurrence of plough effect. It was concluded that the addition of a hard top layer remarkably abated the wear degree of the multilayer ta-C film.

The average wear rates of different multilayer ta-C films and Al_2O_3 counterparts were summarized in Fig. 4. The S1 film was worn through after 4600 cycles, leading to severe wear. The wear rates of the S2 film and the Al_2O_3 counterpart ball were 4.0×10^{-7} mm^3/(N m) and 3.2×10^{-7} mm^3/(N m), respectively. A slightly higher wear rate of 4.8×10^{-7} mm^3/(N m) was observed for the S3 film, and the corresponding Al_2O_3 ball also obtained a much higher wear rate of 5.3×10^{-7} mm^3/(N m). Therefore, the S2 film with a hard top layer exhibited the optimum wear resistance and effectively reduced the wear of Al_2O_3 counterpart at 400 °C, revealing that the composition of the top layer in the multilayer structure controlled the whole wear behavior at high temperature.

The surface morphologies and elemental distributions on the contact region of Al_2O_3 balls were characterized to elucidate the friction mechanism. Fig. 5(a) shows the contact surface of Al_2O_3 ball sliding against the S1 film. The wear scar with a diameter of 189 μm was found, and a lot of wear debris was accumulated around the wear scar. A slight transfer film was also observed in the middle of the wear scar. The EDS mapping revealed that the main component of the wear debris was C element, and the appearance of substrate elements such as W, Co indicated that the S1 film was worn out. For the S2 film, the contact region on the Al_2O_3 counterpart (Fig. 5(b)) exhibited a diminished wear scar with 144 μm in diameter. The surface of the wear scar was quite smooth and free from wear debris. Weak EDS signal of C element suggested a faint transfer layer, and the absence of W and Co elements reflected the high protective efficacy of the S2 film. For the S3 film, the contact area on the Al_2O_3 ball shown in Fig. 5(c) demonstrated that the wear scar had a diameter of 205 μm, and a large number of wear debris appeared in the periphery of the wear scar. A compact transfer film could be found inside the wear scar. The EDS results showed that the main component of the wear debris was C element, and a strong Co signal was observed at the center of the wear scar, indicating the film failure. Consequently, the hard top layer restrained the wear failure of ta-C film and reduced the damage of the friction pair. Moreover, it was worth noting that the wear failure of the S1 film and the S3 film were similarly accompanied by a large number of wear debris and the formation of transfer film on the wear scar, while wear debris and transfer layer failed to be observed on the wear scar of the S2 film with excellent antifriction property and wear resistance. Thus, it was proposed that the emergence of wear debris and transfer film deteriorated the high temperature friction properties.

Fig. 6 shows the optical images of wear tracks on the multilayer ta-C films and wear scars on the Al_2O_3 counterpart. The S1 film suffered severe damage in the contact area with a wide wear track (Fig. 6(a)). Deep grooves and local peeling were observed in the middle of the wear track and at the edge of the wear track, respectively. The corresponding wear scar was large, and abundant black wear debris appeared around the wear scar (Fig. 6(d)). Some furrows were also found inside the wear scar. In contrast, the S2 film obtained a faint wear track (Fig. 6(b)) and a small wear scar (Fig. 6(e)). The contact region possessed a smooth surface and no wear debris was found. However, enlarged wear track and wear scar were noticed for the S3 film. Partial spalling was observed in the wear track (Fig. 6(c)), and the accumulation of black debris occurred around the wear scar (Fig. 6(f)). The results of optical images were in good accordance with those of SEM.

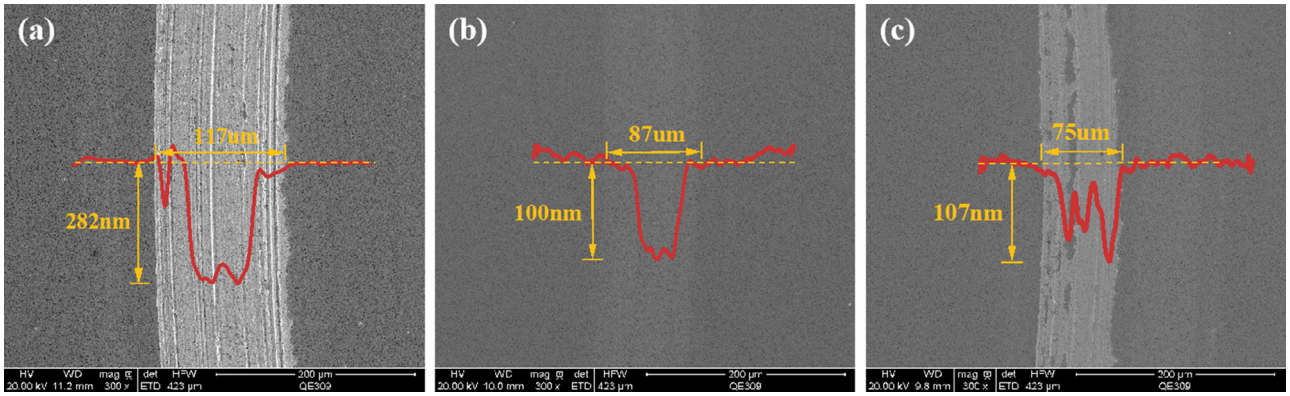

Fig. 3. Surface morphologies and cross-section profiles of (a) S1, (b) S2, (c) S3.

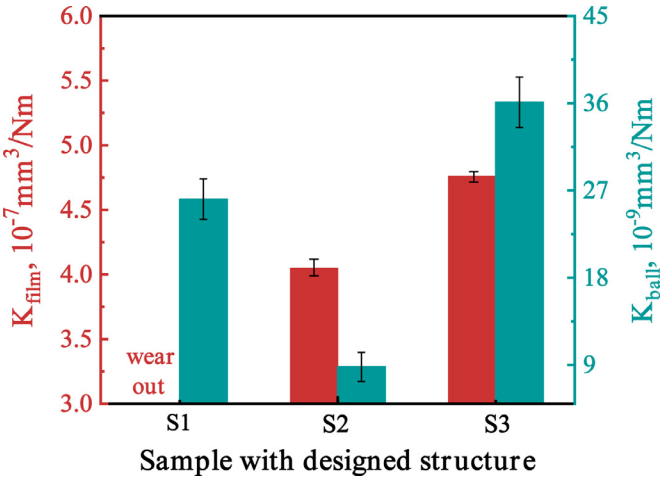

Fig. 4. Wear rates of different multilayer ta-C films and Al_2O_3 counterparts.

The typical positions on wear tracks and wear scars were characterized by Raman spectroscopy to analyze the friction mechanism. As shown in Fig. 6, position A, B, C and D represents the outside of the wear track, the middle of the wear track, the wear debris and the center of the wear scar, respectively. Fig. 7 shows the Raman spectra at different positions of wear tracks and wear scars. The as-deposited films were used as contrast samples. The comparison of positions A and the as-prepared films suggested that the heating at 400 °C in air exerted little influence on the atomic bonds of the multilayer ta-C film. For region B, the Raman signal of the S1 film changed significantly, and the characteristic peak of amorphous carbon appeared to be widened, while the Raman spectra of the S2 film and the S3 film differed a little. Hence, it was inferred that the hard/soft top layer enhanced the stability of carbon bonding structure in the friction contact area. For region C, all the films exhibited two discrete peaks of amorphous carbon, indicating that region C was rich in sp^2 carbon bonds. For region D, Raman signal of amorphous carbon was weakly detected for the S2 film, while typical Raman signals of amorphous carbon located at 1000–2000 cm^{-1} were observed in the S1 and S3 film, indicating that the wear debris was comprised of sp^2-rich amorphous carbon.

The Raman spectra were decomposed into two peaks, namely D peak and G peak, by Gaussian fitting to analyze the atomic bonds of the multilayer ta-C films. The D peak located at 1380 cm^{-1} and G peak located at 1560 cm^{-1} were ascribed to the breathing vibration and stretching vibration of the sp^2 carbon bonds, respectively. The I_D/I_G value, defined as the area ratio of two peaks, could be conducive to clarify the friction mechanism. A higher I_D/I_G ratio suggests an amorphous carbon matrix with larger sp^2 cluster and enhanced bonding order [27,28]. Accordingly, a high sp^2 content could be qualitatively inferred by a high I_D/I_G ratio. Thus, the increased I_D/I_G value after friction could be interpreted as an intensified graphitization degree. Fig. 8 shows the I_D/I_G values of the as-deposited film and different positions of wear tracks and wear scars. For all the films, the I_D/I_G value outside the wear track differed a little with that of the as-deposited film, indicating that the heating at 400 °C in air had little influence on the carbon bonding structure of the designed multilayer ta-C film. For the S1 film, the I_D/I_G value in the middle of the wear track increased significantly to 1.83 compared with that of 0.77 outside the wear track. This change in bonding structure could stem from the sliding triggered graphitization. Meanwhile, the debris around the wear scar and the center of wear scar obtained an I_D/I_G value of 3.72 and 1.61, respectively, which revealed that the multilayer ta-C film in the contact region experienced graphitization transformation and sp^2-rich carbon transfer film and wear debris were formed on the Al_2O_3 counterpart. For the S2 film, the I_D/I_G value in and outside the wear track nearly unchanged, and the I_D/I_G value of the wear debris was 1.25. The weak signal of amorphous carbon in the middle of the wear scar indicated that transfer film was barely formed. For the S3 film, the I_D/I_G values in and outside the wear track were also basically the same. However, wear debris with high I_D/I_G value of 3.12 was formed, and the center of wear scar obtained an increased I_D/I_G value of 1.20 compared to that of S2 film. The above Raman analysis suggested that adding a hard/soft top layer attenuated the friction induced graphitization in the contact region of the multilayer ta-C film. The soft top layer promoted the formation of sp^2-rich carbon wear debris and carbonaceous transfer film, while the hard top layer restrained the graphitized carbon both on the wear track and the wear scar.

For the friction tests conducted at 400 °C, the multilayer ta-C film exhibited limited friction life and quickly worn out, while the addition of a top layer effectively regulated its friction behavior. It should be noted that the multilayer structure with alternating hard and soft sub-layers provided a vital foundation for the superior friction properties under high temperature. The as-prepared multilayer ta-C acted as an important role in stress relaxation and guaranteed a good adhesion between the substrate and the top layer. More importantly, many interfaces and soft sub-layers were embedded in the multilayer structure, which endowed multilayer ta-C film with excellent mechanical properties. Introduction of a hard or soft top layer could modify the friction performance of the total system. Results showed that a hard top layer contributed to superior lubrication effect and wear resistance at 400 °C, while a soft top layer displayed a high friction coefficient. At room temperature, the soft amorphous carbon film was prone to peel off under

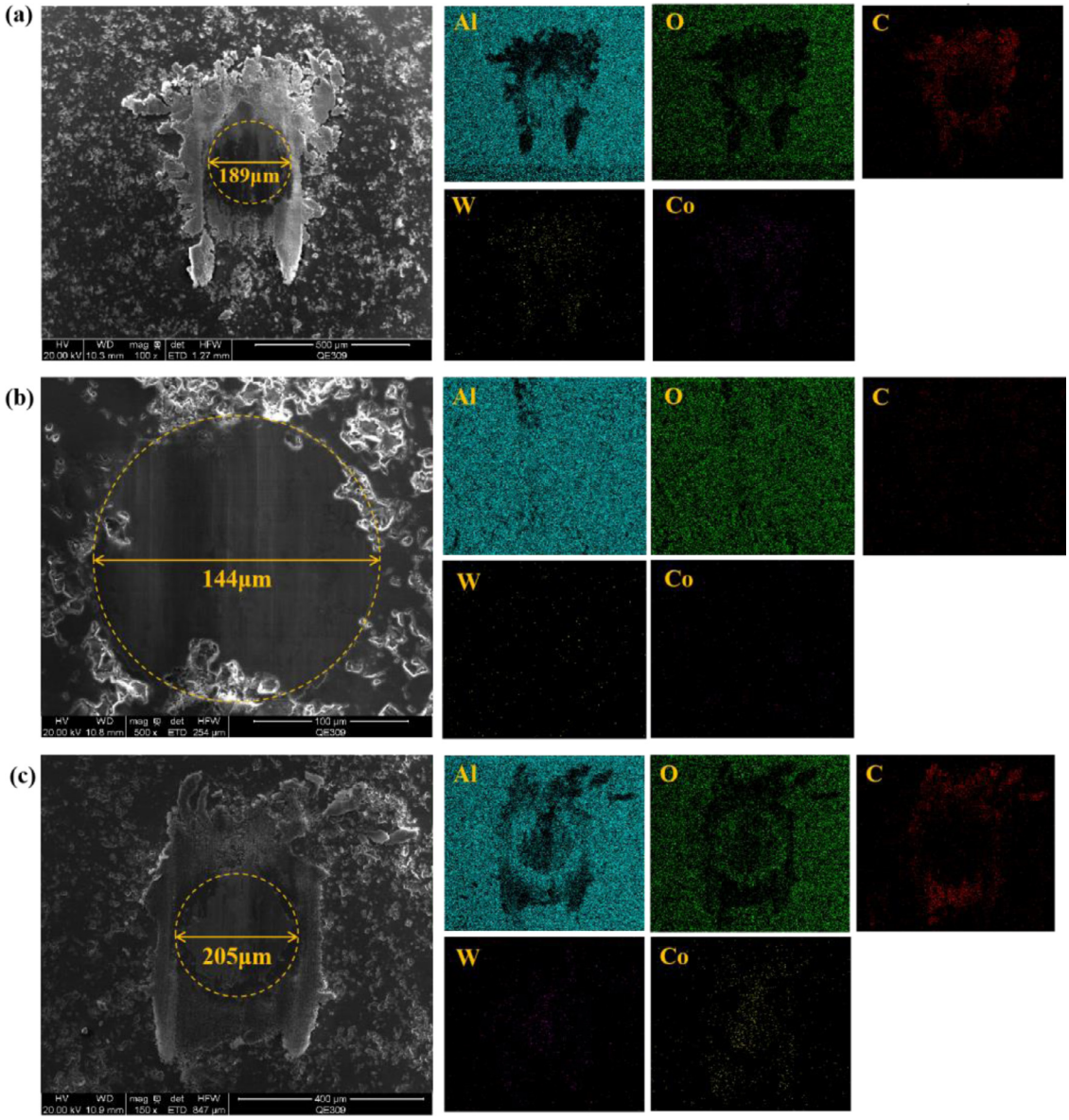

Fig. 5. Surface morphologies and EDS energy spectra of the wear scars for (a) S1, (b) S2, (c) S3.

the action of friction shear, thus forming a graphitized transfer film to reduce the friction coefficient [29–31]. Moreover, the multilayer amorphous carbon film with soft top layer was verified to present superior antifriction and wear resistance under high contact stress compared to that of multilayer film with hard top layer [16], which was inconsistent with the results under high temperature in this work.

In our work, the multilayer ta-C film with hard top layer presented superior friction performance at high temperature (Fig. 4). Graphitization transformation was hardly observed in the middle of the wear track, and carbon transfer film was barely detected in the middle of the wear scar (Fig. 8). Therefore, it was the passivation of carbon dangling bonds at the sliding interface instead of the friction-induced graphitization dominated the low-friction mechanism of the ta-C film at high temperature. More importantly, the sp^2-rich carbon transfer film appeared in the wear scar of the multilayer ta-C film with soft top layer (Fig. 7), which accompanied by a high friction coefficient (Fig. 2). These results indicated that the graphitization and carbon transfer film exerted unfavorable effects on the antifriction and lubrication of ta-C film at high temperature. Moreover, the production of graphitized debris (Fig. 6) could exhaust the ta-C film in the contact area during friction, which gradually resulted in lubrication failure. In addition, the load-bearing capacity of the top layer may play a certain role. The as-prepared multilayer ta-C benefited a high hardness of 54.6 GPa, while the addition of a hard or soft top layer resulted in slight changes of hardness at 56.1 GPa and 51.9 GPa, respectively (as shown in Table S1 in the Supporting Information). Noted that despite of the tiny changes in hardness, the hard top layer with improved hardness could improve the load-bearing capacity of the film and diminish the contact area during friction, which consequently benefitted the low-friction behaviors.

Multiple molecular dynamics simulations have revealed the contact dynamics and interface chemistry of the amorphous carbon film during friction and wear from the nanoscale. The localized shear effect during the sliding could trigger the sp^3 to sp^2 rehybridization [29]. Furthermore, the transition of the local stress from highly compressive to tensile could also drive the sp^3-to-sp^2 transformation [32]. It was inferred that the friction-induced structural evolution, especially the transformation of sp^3-to-sp^2 bond-

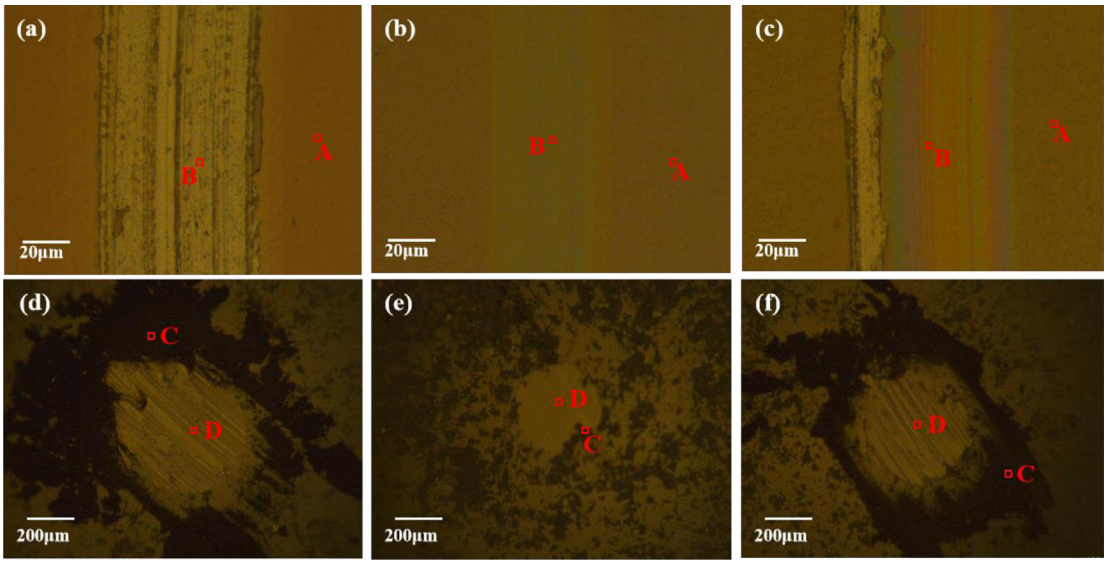

Fig. 6. Optical images of wear tracks and wear scars of (a, d) S1, (b, e) S2, (c, f) S3 (The squares indicate the positions for Raman analysis).

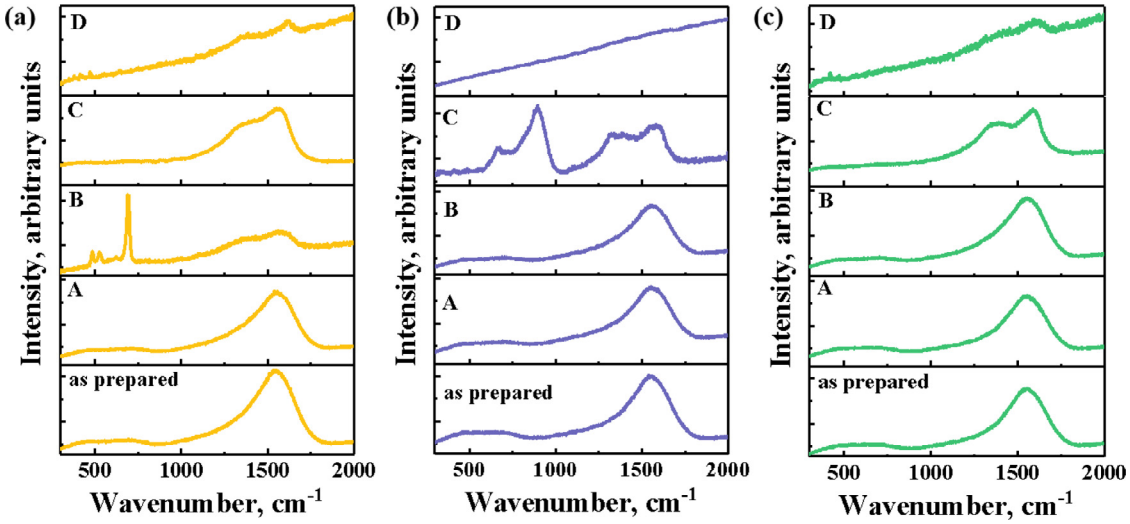

Fig. 7. Raman spectra at different positions of wear tracks and wear scars for (a) S1, (b) S2, (c) S3.

ing states and the formation of sp^2-rich transfer layer, activated the sliding interface. The tribochemical reaction could occur between a sp^2 carbon atom and a radical-containing carbon atom under continued sliding, leading to the formation of a covalent bond [33–35]. Therefore, a high portion of sp^2-bonded carbon at the interface would contribute to high friction force and severe wear due to the remarkable adhesion interactions. Moreover, the tensile stress stemmed from the inhomogeneous contact during the friction could also induce the formation of interfacial C–C bonds between the unsaturated sp^2-bonded carbon atoms, resulting in a high-friction behavior [36]. Thus, the friction induced sp^3-to-sp^2 transformation and the formation of graphitized transfer layer promoted the tribochemical reaction and deteriorated the friction properties of ta-C film at high temperature.

In summary, the friction mechanism of the multilayer ta-C films at 400 °C was described in Fig. 9. The S1 film with alternating hard and soft sublayers performed well before the sudden failure, due to the good mechanical properties and thermal stability of ta-C. Under the continual action of friction shear force, the S1 film in the contact region was gradually consumed. The exfoliated ta-C film could experience the friction induced graphitization and transfer to the Al_2O_3 counterpart, forming abundant wear debris. Once the S1 film worn through, the friction coefficient increased abruptly. For the S2 film, the hard top layer provided sufficient load-carrying capacity and wear resistance during the friction process, thus decreasing the generation of wear debris and the depletion of film. Moreover, the robust sp^3 bonded carbon restricted the graphitization transformation, which attenuated the adhesion force at the sliding interface. The unpaired dangling bonds on the sp^3-rich ta-C surface were effectively passivated by the active species in the atmosphere, which resulted in the weak interaction with the inert Al_2O_3 counterpart. These combined factors accounted for the superior friction properties of the S2 film at high temperature. For the S3 film, the soft top layer offered limited mechanical properties and inadequate load-carrying capacity, leading to enlarged contact area and severe friction action. Meanwhile, the poor wear resistance of the sp^2-rich top layer promoted the formation of wear debris and graphitized transfer layer. The active C–C sp^2 carbon

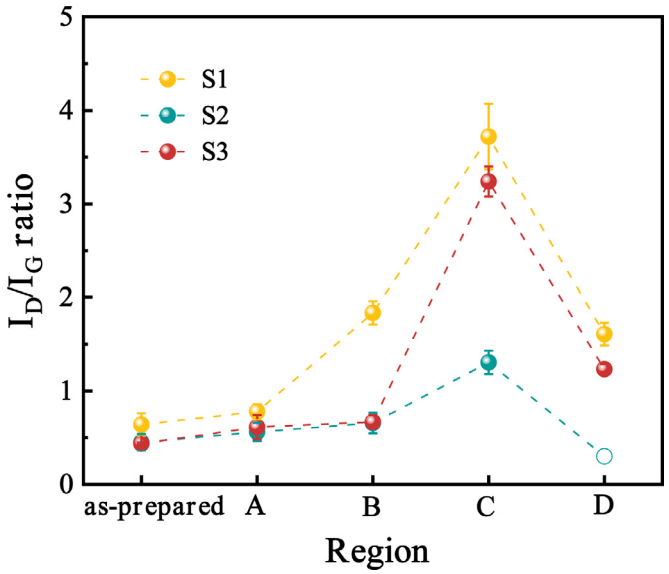

Fig. 8. I_D/I_G values of as-deposited film and different positions of wear tracks and wear scars.

bonds interacted severely with the graphitic transfer layer formed on the counterpart at high temperature, resulting in severe adhesive interaction and undesirable friction behavior.

In order to further explore the high-temperature friction mechanism, the friction tests of the S2 film were carried out at different temperatures. Fig. 10(a) shows the friction curves at different temperatures. The run-in periods of friction were observed at all temperatures. The S2 film obtained a stable low friction coefficient of 0.11 at 400 °C. When the test temperature increased to 500 °C, the friction coefficient of the S2 film still remained at a low value of 0.12, but the friction curve exhibited a certain fluctuation. As the temperature reached 600 °C, the friction coefficient increased rapidly at 1600 cycles, indicating that the S2 film was worn through. Fig. 10(b) shows the optical images after friction tests. The S2 film remained intact without visible surface damage after the friction test at 400 °C and 500 °C, while serious damage of the film was observed after the friction test at 600 °C, which indicated that the critical thermal stable temperature of the S2 film was below 600 °C. High temperature could induce the transformation of sp^3 bonded carbon into sp^2 bonded carbon in ta-C film, resulting in the decreased hardness. Moreover, the high temperature oxidation could bring fatal damage to the ta-C film.

The post-annealing treatment of the S2 film at 400, 500 and 600 °C for 30 min was conducted to shed light the failure mechanism. The hardness of the S2 film after annealing at 400 °C and 500 °C was 54.3 GPa and 53.8 GPa, respectively, which was slightly different from the 56.1 GPa of as-prepared film (as shown in Table S2). However, a low hardness of 13.5 GPa was observed after annealing at 600 °C, indicating the severe damage of the S2 film.

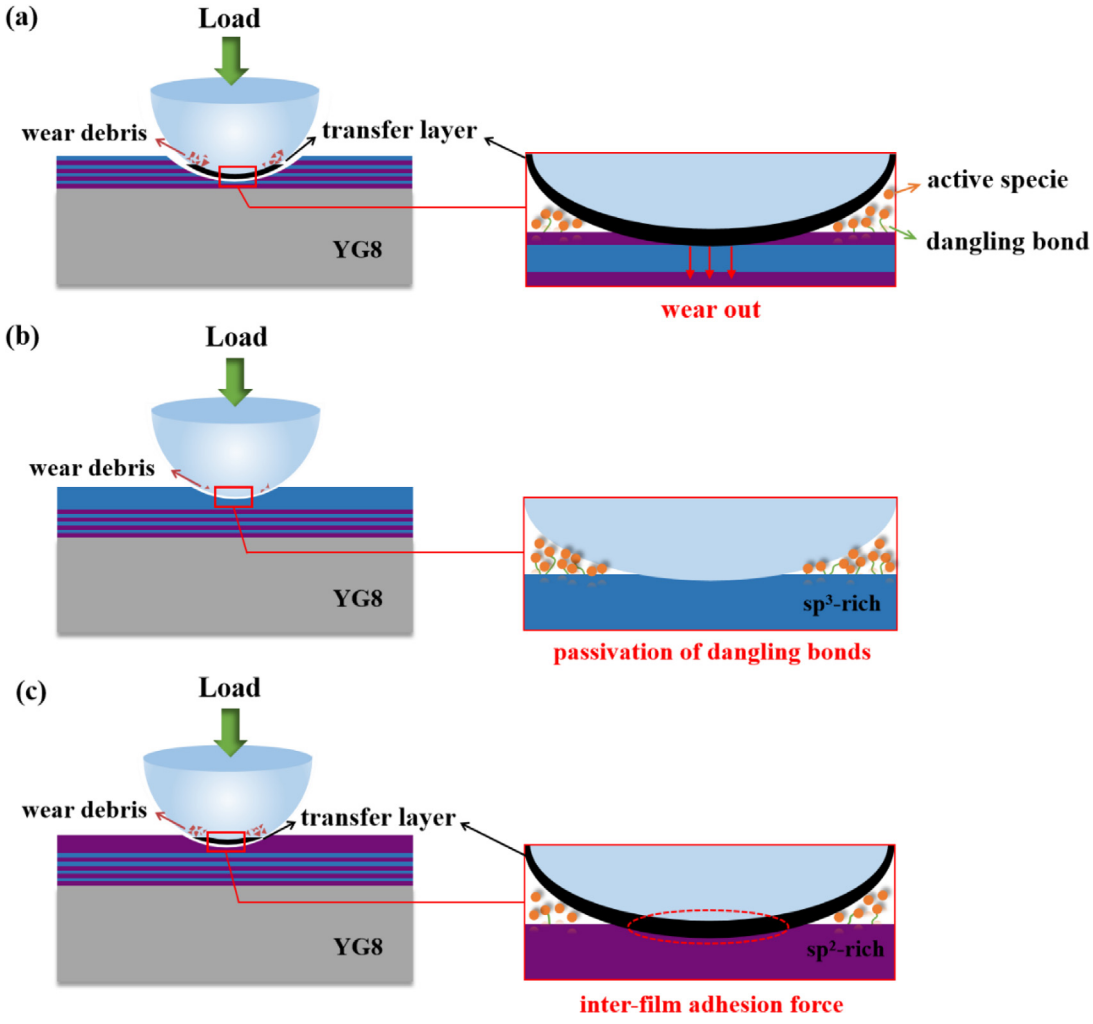

Fig. 9. Schematic diagrams of wear mechanism of the designed multilayer ta-C films S1, (b) S2, (c) S3.

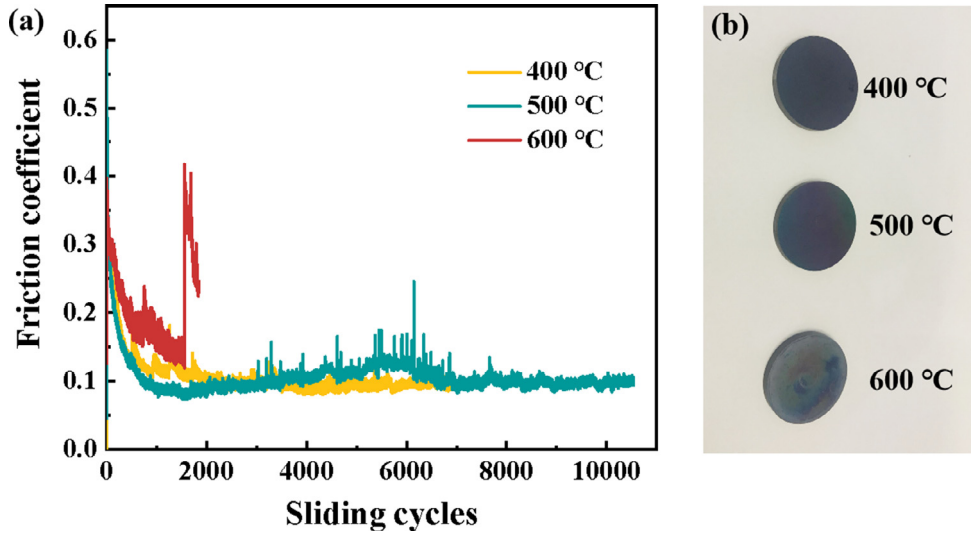

Fig. 10. (a) Friction curves of S2 at different test temperature; (b) optical images after friction tests.

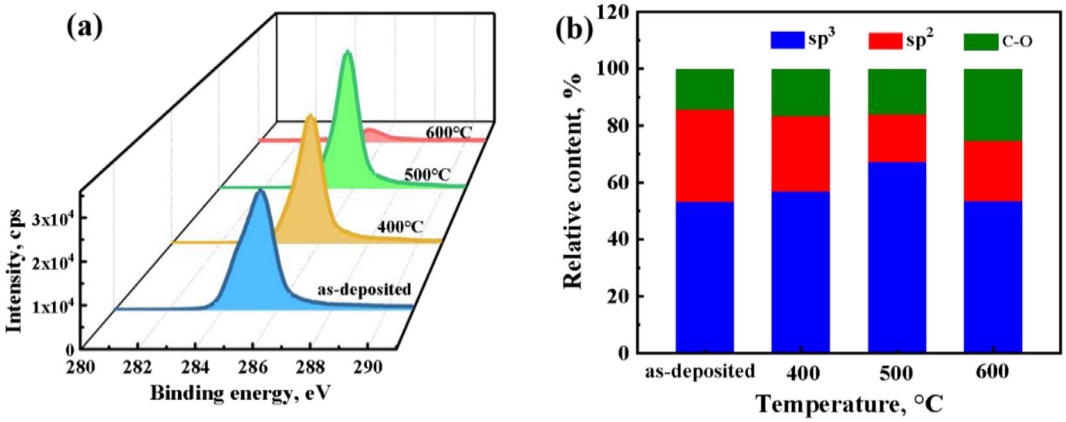

Fig. 11. (a) The XPS C 1s spectra of the as-prepared and annealed S2 film, (b) the relative content of sp^3, sp^2 and C–O fractions acquired from peak-fitting.

The evolution of chemical composition and carbon atomic bonds were analyzed by XPS tests. Fig. 11(a) shows the XPS C 1s spectra of the as-prepared and annealed S2 film. The peak positions and peak intensities were summarized in Table S3. When the S2 film was annealed at 400 °C and 500 °C, the binding energy of the C 1s peak gradually increased to 285.7 eV and 285.8 eV compared to 285.4 eV of the as-prepared film, while the peak intensity showed non-dependence on temperature. Since the binding energy of sp^3-hybrided carbon atom was higher than sp^2-hybrided carbon atom [37], it could be concluded that the up-shift of the C 1s peak was possibly ascribed to the enhanced proportion of sp^3-bonded carbon. However, the C 1s peak down-shifted to 285.3 eV and the peak intensity was reduced by an order of magnitude after annealing at 600 °C, suggesting that the S2 film was partially volatilized from the substrate. In addition, different with the stable atomic percentages of C and O elements within 500 °C, the C atomic percentage sharply decreased and the proportion of oxygen atoms substantially increased in case of annealing temperature at 600 °C (as shown in Table S3), indicating the severe oxidation of the S2 film. The C 1s spectra were deconvolved into three peaks, namely C–C sp^2 bond located at 284.3 ± 0.2 eV, C–C sp^3 bond located at 285.2 ± 0.2 eV and C–O bond located at 286.5 ± 0.3 eV. The relative content of the different carbon bonds was calculated by the area ratio. Fig. 11(b) shows the evolution of relative content of sp^3 carbon bonds, sp^2 carbon bonds and C–O bonds with annealing temperature. In contrast to the as-deposited film, annealing at 400 °C and 500 °C promoted the C–C sp^3 bonds and reduced the C–C sp^2 bonds. This counterintuitive result could be attribute to the fact that the thermal stability of the C–C sp^3 bonds was superior to the C–C sp^2 bonds. Hence, the C–C sp^2 bonds was preferentially oxidized at high temperature, leaving the robust C–C sp^3 bonds. Beyond 600 °C, the content of C–O bond increased evidently, while the percentage of sp^3 carbon bond diminished, indicating that the critical thermal stable temperature of the C–C sp^3 bond was lower than 600 °C.

According to the results of post-annealing treatment, it was inferred that the degraded friction performance of the multilayer ta-C film at 600 °C was mainly due to the oxidation and volatilization of carbon atoms induced by the high temperature. At the same time, friction may accelerate the oxidation failure of ta-C film.

4. Conclusion

The high temperature friction behaviors of the ta-C films with different multilayer structures were systematically analyzed. Results revealed that the top layer of the multilayer structure dominated the high temperature friction performance of the ta-C film. A hard top layer contributed to superior lubrication effect and wear resistance at 400 °C, while a soft top layer deteriorated the friction properties. The low-friction mechanism of the ta-C film at high temperature was proposed to be dominated by the passivation of carbon dangling bonds at the sliding interface. However,

the friction-induced structural evolution, especially the transformation of sp^3-to-sp^2 bonding states and the formation of sp^2-rich carbon transfer layer, induced strong C–C bonding interaction at the sliding interface and thus led to the deteriorated friction behaviors. The multilayer ta-C film with a hard top layer maintained desirable friction properties below 500 °C, while the degraded friction behavior at 600 °C was mainly ascribed to the oxidation and volatilization of carbon atoms induced by the extra-high temperature.

Declaration of Competing Interest

We have no conflicts of interest to this work.

Acknowledgements

The present research was funded by The National Science Fund for Distinguished Young Scholars of China (No. 52025014), National Science and Technology Major Project (No. 2017-VII-0012-0108), K.C. Wong Education Foundation (No. GJTD-2019-13), CAS Interdisciplinary Innovation Team (No. 292020000008), Ningbo Science and Technology Innovation Project (No. 2018B10012).

Supplementary materials

Supplementary material associated with this article can be found, in the online version, at doi:10.1016/j.jmst.2021.04.028.

References

[1] M. Rubner, Nature 423 (2003) 925–926.
[2] X.D. Li, W.C. Chang, Y.J. Chao, R.Z. Wang, M. Chang, Nano Lett. 4 (2004) 613–617.
[3] X. Han, J. Zhu, J. Han, M. Tan, Z. Jia, C. Jiang, Appl. Surf. Sci. 255 (2008) 607–609.
[4] S. Logothetidis, S. Kassavetis, C. Charitidis, Y. Panayiotatos, A. Laskarakis, Carbon 42 (2004) 1133–1136.
[5] S. Wang, J. Zhu, J. Wang, X. Yin, X. Han, Thin Solid Films 519 (2011) 4906–4909.
[6] D. Sheeja, B.K. Tay, S.P. Lau, X. Shi, X. Ding, Surf. Coat. Technol. 132 (2000) 228–232.
[7] Z. Xu, Y.J. Zheng, F. Jiang, Y.X. Leng, H. Sun, N. Huang, Appl. Surf. Sci. 264 (2013) 207–212.
[8] Y.J. Jo, T.F. Zhang, M.J. Son, K.H. Kim, Appl. Surf. Sci. 433 (2018) 1184–1191.
[9] S. Takabayashi, K. Okamoto, T. Nakatani, Surf. Interface Anal. 50 (2018) 441–447.
[10] M. Rouhani, C.N. Hong, Y.R. Jeng, Carbon 130 (2018) 401–409.
[11] Y. Zhang, Y. Zhai, F. Li, S. Zhang, P. Zhang, S. Zhang, Surf. Coat. Technol. 232 (2013) 575–581.
[12] J. Wei, H. Li, L. Liu, P. Guo, P. Ke, A. Wang, Surf. Coat. Technol. 374 (2019) 317–326.
[13] E.H.T. Teo, D.H.C. Chua, B.K. Tay, Diamond Relat. Mater. 16 (2007) 1882–1886.
[14] Z. Xu, H. Sun, Y.X. Leng, X. Li, W. Yang, N. Huang, Appl. Surf. Sci. 328 (2015) 319–324.
[15] Y. Lin, A.W. Zia, Z. Zhou, P.W. Shum, K.Y. Li, Surf. Coat. Technol. 320 (2017) 7–12.
[16] Y. Lin, Z. Zhou, K.Y. Li, Appl. Surf. Sci. 477 (2019) 137–146.
[17] S. Kundu, N. Dwivedi, N. Satyanarayana, R.J. Yeo, J. Ahner, P.M. Jones, C.S. Bhatia, ACS Appl. Mater. Interfaces 7 (2015) 158–165.
[18] J. Matlak, K. Komvopoulos, Sci. Rep. 8 (2018) 9647.
[19] M. Murakawa, M. Jin, M. Hayashi, Surf. Coat. Technol. 177 (2004) 631–637.
[20] F. Klocke, O. Dambon, M. Rohwerder, F. Bernhardt, M. Friedrichs, S.V. Merzlikin, Int. J. Adv. Manuf. Technol. 87 (2016) 43–49.
[21] X. Deng, H. Kousaka, T. Tokoroyama, N. Umehara, Tribol. Int. 75 (2014) 98–103.
[22] M.Z.U.K.S. Bhowmick, A. Banerji, M.J. Lukitsch, A.T. Alpas, Appl. Surf. Sci. 450 (2018) 274–283.
[23] S. Bhowmick, A. Banerji, M.Z.U. Khan, M.J. Lukitsch, A.T. Alpas, Surf. Coat. Technol. 284 (2015) 14–25.
[24] S. Miyake, S. Suzuki, M. Miyake, Materials 10 (2017) 159.
[25] W. Wang, J. Pu, Z. Cai, S. Zheng, Y. Wei, Vacuum 176 (2020) 109332.
[26] H. Sun, F. Lei, T. Li, H. Han, B. Li, D. Li, D. Sun, ACS Appl. Mater. Interfaces 13 (2021) 6678–6687.
[27] A.C. Ferrari, J. Robertson, Phys. Rev. B 61 (2000) 14095–14107.
[28] A.C. Ferrari, J. Robertson, Philos. Trans. 362 (2004) 2477.
[29] T.B. Ma, L.F. Wang, Y.Z. Hu, X. Li, H. Wang, Sci. Rep. 4 (2014) 3662.
[30] J.D. Schall, G. Gao, J.A. Harrison, J. Phys. Chem. C 114 (2010) 5321–5330.
[31] P. Manimunda, A. Alazizi, S.H. Kim, R.R. Chromik, ACS Appl. Mater. Interfaces 9 (2017) 16704–16714.
[32] T.B. Ma, Y.Z. Hu, H. Wang, Carbon 47 (2009) 1953–1957.
[33] G.T. Gao, P.T. Mikulski, J.A. Harrison, J. Am. Chem. Soc. 124 (2002) 7202–7209.
[34] J.D. Schall, G. Gao, J.A. Harrison, J. Phys. Chem. C 114 (2010) 5321–5330.
[35] X. Li, A. Wang, K.-R. Lee, Carbon 170 (2020) 621–629.
[36] Y. Wang, J. Xu, Y. Ootani, S. Bai, Y. Higuchi, N. Ozawa, K. Adachi, J.M. Martin, M. Kubo, ACS Appl. Mater. Interfaces 9 (2017) 34396–34404.
[37] A.T. Kozakov, A.G. Kochur, N. Kumar, K. Panda, A.V. Nikolskii, A.V. Sidashov, Appl. Surf. Sci. 536 (2021) 147807.